DOI: 10.1002/anie.200802207

Tungsten Photocatalysts

Nanoporous-Walled Tungsten Oxide Nanotubes as Highly Active Visible-Light-Driven Photocatalysts**

*Zhi-Gang Zhao and Masahiro Miyauchi**

Semiconductor photocatalysis is important for many current environmental and energy issues because, in addition to splitting water to supply clean and recyclable hydrogen energy, it can utilize solar energy to decompose harmful organic and inorganic pollutants present in air and aqueous systems.[1–4] TiO_2 is currently the best known and most widely used highly efficient photocatalytic material because it is stable and cheap. However, only a small UV fraction of solar light (3–5%) can be utilized[5,6] due to its wide bandgap, therefore an imperative and challenging issue is to develop new and efficient visible-light-sensitive photocatalysts. Visible-light photocatalysis has recently been reported in nitrogen-doped TiO_2.[7–9] However, nitrogen doping leads to localized states in the bandgap of TiO_2, and the localized holes produced at the impurity level have a slower mobility than those in the valence band. The quantum efficiency of nitrogen-doped TiO_2 under visible light is therefore much lower than that under UV illumination.[8] In contrast, tungsten trioxide (WO_3), which possess a small bandgap of between 2.4 and 2.8 eV, has many advantages for visible-light-driven photocatalysis, including a deeper valence band (+3.1 eV), strong adsorption within the solar spectrum, stable physicochemical properties, and resilience to photocorrosion effects.[10] However, pure WO_3 has a lower light energy conversion efficiency than the more widely used TiO_2 as the reduction potential of the electrons in WO_3 is low due to its low conduction band level. Abe et al. have recently proposed that Pt loading is an attractive solution to enhance the photocatalytic properties because loaded Pt can trap photogenerated electrons from WO_3 to reduce O_2 to H_2O_2.[11]

Nanoscience research can greatly impact the development of new and more potent catalysts by designing and controlling their photocatalytic properties, especially in terms of the energy gap, chemical composition, and surface modification. For example, because photocatalytic activity is closely related to particle diameter and morphology,[12] Bi_2WO_6,[13] $La_2Sn_2O_7$,[14] and $ZnWO_4$[15] nanostructures with different morphologies have been synthesized and their photocatalytic properties explored.

The Pt-loaded nanotubular structure that results from combining the ideas of nanostructural control with a Pt/WO_3 multicomponent composite as a heterocatalyst should therefore be more promising for visible-light-driven photocatalysis. The nanotubular architecture would result in a larger effective surface area and provide more active sites in close proximity to the Pt nanoparticles, thus enabling diffusive transport of photogenerated electrons to these nanoparticles. More importantly, however, the energy band at the surface bends, and the band-bending potential may establish a depletion region at a very short distance from the material's surface. Such a depletion layer would effectively decrease charge–carrier recombination rates and thereby increase the photocatalytic ability.[16] Another possible advantage of a porous structure is that the incident photons are more effectively absorbed than on a flat surface due to light scattering.[16,17]

The synthesis of high-purity WO_3 nanotubes (NTs) is rather rare, especially using a template-free solvothermal method. The use of anodic aluminum oxide (AAO)[18,19] or biological templates[20] may introduce impurities into the WO_3 materials and will in any case complicate the separation process. Moreover, most methods using templates or thermal evaporation techniques are intrinsically expensive and give low yields and purities.[18–21] The development of cheap and template-free methods suitable for the large-scale synthesis of high-purity WO_3 NTs is therefore the primary objective of this work. Choi et al. have reported a simple process for the synthesis of tungsten oxide ($W_{18}O_{49}$) nanorods in ethanol solvent using tungsten hexachloride (WCl_6) as a raw material.[22] Their work has shown that the slow alcoholysis of WCl_6 with ethanol results in the formation of rod-like nanoparticles in an autoclave. This process should follow traditional self-aggregation and Ostwald ripening growth mechanisms. It has also been found recently that urea can be rationally used to assemble organic crystals ranging from one-dimensional chains to nanotubes due to its strong hydrogen-bonding properties.[23] It is therefore plausible that urea could be a suitable ligand or directing agent in an ethanol/WCl_6 system for the synthesis of inorganic tungsten oxide nanostructures as it can act as both a hydrogen-bond donor through its two NH protons or a hydrogen-bond acceptor through the lone pairs of the C=O group.[23] Similarly, protons resulting from the alcoholysis of WCl_6 may adsorb on the surface of the as-prepared nanoparticles during the growth process and interact with urea, thereby also tuning the morphology of the final products.

[*] Dr. Z.-G. Zhao, Dr. M. Miyauchi
Nanotechnology Research Institute
National Institute of Advanced Industrial Science and Technology
Tsukuba Central 5, 1-1-1 Higashi, Tsukuba, Ibaraki, 305-8565 (Japan)
Fax: (+81)-29-861-6299
E-mail: m-miyauchi@aist.go.jp
Homepage: http://staff.aist.go.jp/m-miyauchi/

[**] This work was supported by the New Energy and Industrial Technology Development Organization (NEDO) and was partly conducted in the AIST Nano-Processing Facility, which is supported by the "Nanotechnology Support Project" of the Ministry of Education, Culture, Sports, Science and Technology of Japan.

Supporting information for this article is available on the WWW under http://dx.doi.org/10.1002/anie.200802207.

Herein we report the first example of a facile and cheap synthesis of Pt-loaded nanoporous-walled WO_3 NTs by template-free urea-assisted alcoholysis of WCl_6 and subsequent calcination. These NTs were subsequently found to be promising visible-light-driven photocatalysts. Gas-phase acetaldehyde decomposition was used as a probe reaction to evaluate the photocatalysis of the Pt-loaded WO_3 NTs and their activity was compared to Pt-loaded commercial WO_3 nanoparticles and nitrogen-doped TiO_2 nanoparticles under visible light (> 430 nm) illumination. The amount of loaded Pt was adjusted to determine the optimal concentration of Pt loading for photocatalytic activity. It was found that the photocatalytic activity of Pt-loaded WO_3 NTs is superior to that of Pt-loaded commercial WO_3 nanoparticles and nitrogen-doped TiO_2 under these conditions.

Figure 1 illustrates the principal steps involved in this synthesis. The process begins with the synthesis of tungstic acid hydrate (protonated tungsten oxide, $H_2W_{1.5}O_{5.5}\cdot H_2O$) NTs using a template-free approach in which WCl_6 is treated solvothermally in ethanol in the presence of urea. Platinum nanoparticles with diameters of 2–4 nm were obtained by the well-known citrate method using H_2PtCl_6 as a starting material.[24] The as-synthesized tungstic acid hydrate NTs and Pt nanoparticles were mixed with specific compositions and the mixture stirred before slow calcination at 450 °C. The obtained Pt-loaded WO_3 NTs were used as photocatalysts for gas-phase acetaldehyde decomposition.

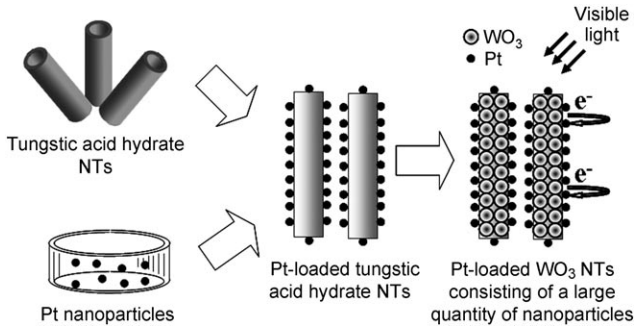

Figure 1. Fabrication of Pt-loaded WO_3 NTs.

The X-ray diffraction (XRD) patterns shown in Figure 2 are for samples obtained from the solvothermal reaction (curve a) and after calcination (curve b). The product of the solvothermal reaction was identified as crystalline tungstic acid hydrate (space group: $Fd\bar{3}m$ (no. 227); JCPDS No. 48-0719). The calculated lattice constants ($a = b = c = 10.1$ Å) are close to the theoretical value of 10.21 Å. The tungstic acid hydrate phase transformed into tungsten trioxide upon calcination, as confirmed by the presence of three characteristic peaks in the $23° < 2\theta < 25°$ range in the XRD pattern. All the peaks in this pattern could be indexed as pure triclinic tungsten trioxide (space group: $P\bar{1}$ (no. 2)) with calculated lattice constants of $a = 7.32$, $b = 7.57$, $c = 7.55$ Å and $\alpha = 89.11°$, $\beta = 90.02°$, $\gamma = 90.78°$ (JCPDS No. 20-1323). No peaks arising from tungstic acid or other phases were detected in the spectrum, thus suggesting that the impurities in the product after calcination are lower than the detection limit of XRD. The observed broadening of the diffraction peaks was ascribed to the very small crystallite size within the NTs.

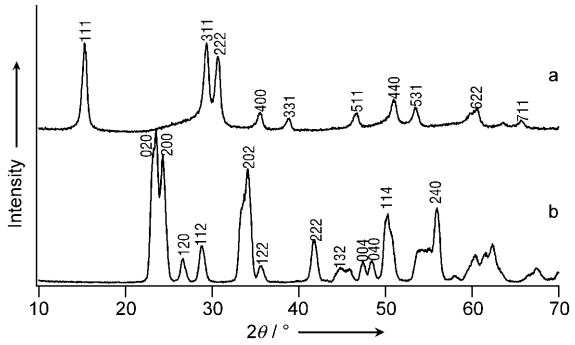

Figure 2. XRD patterns of a) tungstic acid hydrate before calcination and b) tungsten oxide NTs after calcination.

The structural details of tungstic acid hydrate and the tungsten trioxide NTs were investigated using a scanning electron microscope (SEM) and a transmission electron microscope (TEM). Figure 3a shows a low-magnification SEM image of a sample obtained from the solvothermal reaction, which is composed of a large quantity of well-dispersed NTs with outer diameters of 300–1000 nm and lengths of 2–20 μm. Figures 3b and c are high-magnification SEM images of tungstic acid hydrate NTs. Figure 3b shows that the tungstic acid hydrate NT has a nearly rectangular pore of around 250 nm. The surface of the NTs is not smooth (Figure 3c), thus indicating that the NTs are polycrystalline. Figure 3d shows a group of fully calcined NTs (450 °C, 3 h) with the same tubular structure and overall dimensions as their precursor NTs. These calcined NTs are free-standing

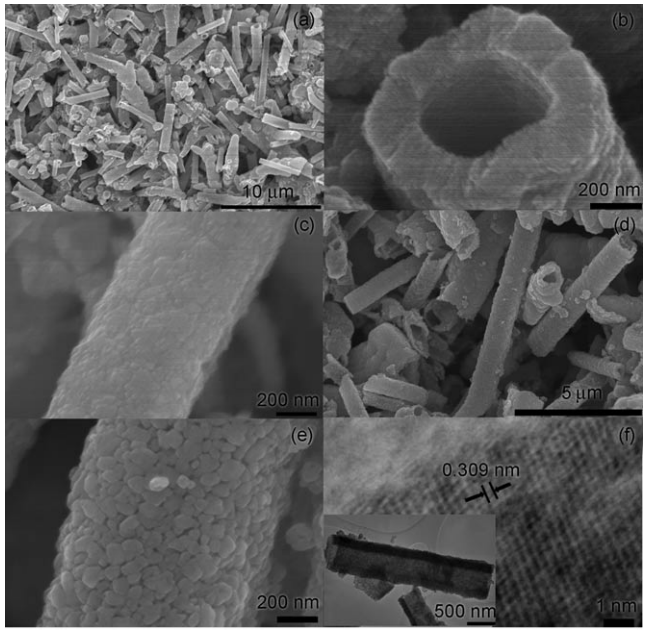

Figure 3. SEM images of NTs before (a–c) and after annealing (d,e); f) high-magnification TEM image. The inset in (f) shows the TEM image of a single NT after annealing.

and show no signs of aggregation after calcination. Moreover, Figure 3e clearly demonstrates that the annealed NT walls consist of individual nanoparticles arranged one-dimensionally and that numerous self-supported pores are formed by the incomplete aggregation of nanoparticles. The sidewalls of the nanotubes are therefore porous. Although the diameter of the nanoparticles is approximately 40–80 nm, the nanotubes are still 2–20 μm long. A representative high-resolution TEM (HRTEM) image of a single WO_3 NT shown in Figure 3f shows that the lattice fringes of the nanocrystals in this NT have a spacing of 0.309 nm, which corresponds well to the interplanar distance of the (112) plane of triclinic tungsten trioxide. The inset demonstrates that the NT is open at both ends.

Nitrogen cryosorption studies, which clearly revealed the existence of mesopores and macropores in the WO_3 NTs, were conducted to investigate the porosity. Commercial WO_3 particles were found to have only a low BET surface area of 4.4 $m^2 g^{-1}$, whereas the specific surface area of our WO_3 NTs was determined to be 25 $m^2 g^{-1}$. This value is more than 5.7 times larger than that of commercial WO_3 particles (see Figure S1a in the Supporting Information). The nitrogen absorption isotherm of the NTs exhibits type II/III characteristics. Figure S1b in the Supporting Information shows the pore-size distribution. The NTs predominantly contains pores in the range 10–60 nm (mesopores and macropores) whose size is attributed to the porous sidewalls. The pores from the tubular structure cannot be seen because the inner diameter of the NTs (300–600 nm) is beyond the measurement range. The pore-size distribution of tungstic acid hydrate NTs before annealing (Figure S1c in the Supporting Information) reveals the absence of mesopores and macropores. The pores in the sidewalls of the NTs must therefore be formed during annealing without destroying the tubular structure. These mesopores and macropores may be suitable to accommodate 2–4-nm Pt nanoparticles. The UV/Vis spectra of our NTs indicated that they have a bandgap of 2.6 eV and that they can absorb visible light with a wavelength above 400 nm (Figure S2 in the Supporting Information).

The NTs were examined in the photocatalytic degradation of acetaldehyde after Pt loading, as described in the Experimental Section. The photoactivity of the NTs was evaluated by measuring the decrease in acetaldehyde and the production of CO_2 in the gas phase upon visible-light irradiation. Figures 4a and b (incident visible light intensity: 20 $mW cm^{-2}$; initial acetaldehyde concentration: about 500 ppmv) show typical plots of the decrease in acetaldehyde concentration and the increase in CO_2 concentration as a function of irradiation time. The reaction vessel was kept in the dark for one hour before analysis to ensure adsorption/desorption equilibrium. The amount of acetaldehyde adsorbed on the commercial WO_3 particles at equilibrium was only about 5–10% of the gas-phase acetaldehyde in the reaction vessel; however, it was about 15–30% for the as-prepared WO_3 NTs. These observations confirm that the WO_3 NTs have a larger effective surface area than commercial WO_3 particles.

The photocatalytic activity of WO_3 NTs is better than that of commercial WO_3 particles at each Pt-loading concentration, as shown in Figures 4a and b. The activity of WO_3 NTs is also superior to that of nitrogen-doped TiO_2 particles. To enable a quantitative comparison, the decomposition rates for the first 30 min were proposed to represent the photocatalytic activities because this region is most likely to be dominated by pure light-intensity-limited conditions.[25] Figure 4c shows these values and clearly indicates that 0.5 wt% Pt-loading produces the most effective photocatalytic reactivity for both WO_3 NTs and commercial nanoparticles. An excessive Pt loading can decrease the photocatalytic activity due to photon absorption by the photocatalytically inactive Pt nanoparticles. The photocatalytic reactivity of 0.5 wt% Pt-loaded WO_3 NTs

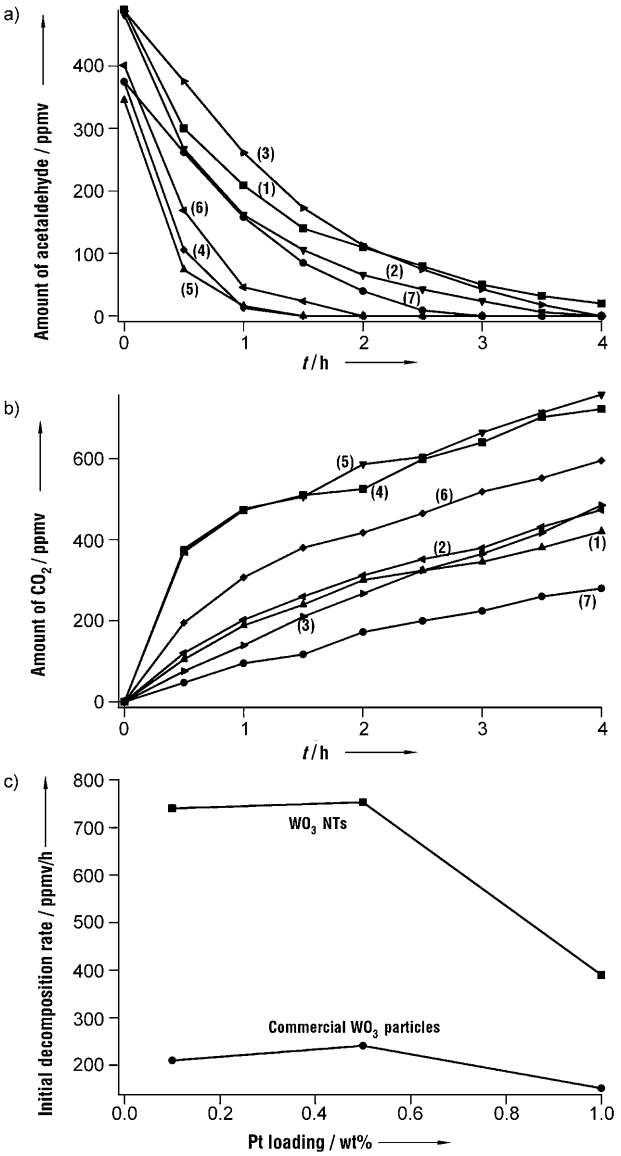

Figure 4. Plots of a) the decrease in acetaldehyde concentration and b) the increase in CO_2 concentration vs. irradiation time during the photocatalytic degradation of about 500 ppmv acetaldehyde by 0.1 wt% Pt-loaded WO_3 commercial particles (1), 0.5 wt% Pt-loaded WO_3 commercial particles (2), 1 wt% Pt-loaded WO_3 commercial particles (3), 0.1 wt% Pt-loaded WO_3 NTs (4), 0.5 wt% Pt-loaded WO_3 NTs (5), 1 wt% Pt-loaded WO_3 NTs (6), and nitrogen-doped TiO_2 (7); c) initial decomposition rates vs. Pt-loading concentration.

upon irradiation with visible light is about three and eight times greater than that of 0.5 wt% Pt-loaded commercial particles and nitrogen-doped TiO_2, respectively. Such a large activity enhancement probably arises from the unique tubular structure, which results in a larger effective surface area, a higher mobility of the charge carriers in the depletion region, and larger numbers of photons adsorbed by light scattering.[16,17]

We confirmed the complete decomposition of acetaldehyde to CO_2 on NTs—the concentration of CO_2 generated when irradiating with visible light reached about 1000 ppmv (Figure S3 in the Supporting Information), while only incomplete decomposition was observed for undoped WO_3 NTs (Figure S4 in the Supporting Information). Tungstic acid hydrate NTs showed no photocatalytic activity upon irradiation with visible light. The photocatalytic activity of pure WO_3 NTs in the initial four hours was inferior to that of Pt-loaded WO_3 NTs. The apparent quantum yields (QY) for 0.5 wt% Pt-loaded WO_3 NTs, 0.5 wt% Pt-loaded commercial WO_3 particles, and nitrogen-doped TiO_2 were calculated to be 1.03%, 0.24%, and 0.22%, respectively. The QY for 0.5 wt% Pt-loading WO_3 NTs is therefore about four times that of 0.5 wt% Pt-loaded commercial WO_3 particles and nitrogen-doped TiO_2 and is similar to that of TiO_2 under UV illumination.[25]

To explore a plausible mechanism for the enhanced photocatalytic ability of Pt-loaded WO_3 NTs, the Pt-loaded NTs were observed by TEM (Figure S5 in the Supporting Information). These NTs were found to be composed of nanoparticles with sizes of between 40 and 80 nm. Nanopores were visible between the WO_3 nanoparticles, which may be useful for Pt loading as they can act as Pt-buffering reservoirs for the incorporation of Pt nanoparticles. Figure S5b (Supporting Information) shows that most Pt particles are rather small (2–4 nm) and are preferentially located in the nanopores, whereas Pt particles can only be deposited on the outer surface of commercial WO_3 particles. The porous tubular structure is therefore expected to enhance the contact between the Pt particles and WO_3 and thereby increase the photocatalytic activity.

In summary, we have developed a facile and economical method to produce high-purity tungstic acid hydrate NTs and nanoporous-walled WO_3 NTs on a large scale. These WO_3 NTs are monodisperse, around 300–1000 nm in diameter and 2–20 μm in length, and are formed by a linear arrangement of individual WO_3 nanoparticles as building blocks. These NTs possess larger specific surface areas than commercial WO_3 particles. The UV/Vis spectrum confirms that these NTs can absorb visible light above a wavelength of 400 nm; the estimated bandgap value is 2.6 eV. After Pt loading, the NTs show a higher photocatalytic activity for the degradation of gas-phase acetaldehyde than commercial WO_3 particles and nitrogen-doped TiO_2. Such a large activity enhancement probably arises from the unique tubular structure, which results in a larger effective surface area, higher mobility of the charge carriers, and more adsorbed photons. This work provides a new route for the design of muliticomponent photocatalysts with improved photocatalytic activity as well as a new material for use in solar cells, nanodevices, and other applications.

Experimental Section

Preparation of tungstic acid hydrate nanotubes: WCl_6 (0.397 g, 1 mmol) and urea (0.6 g, 10 mmol) were added to 40 mL of absolute ethanol. The mixture was loaded into a Teflon-lined autoclave, which was then sealed, maintained at 180 °C for 12 h, and then allowed to cool to room temperature. The resulting white precipitate was collected and rinsed several times with distilled water and absolute ethanol. It was then dried at 60 °C for 12 h.

Preparation of colloidal platinum solution: Sodium citrate solution (1 wt%, 16 mL) was added to a 0.1 wt% H_2PtCl_6 solution (50 mL) with vigorous stirring and the mixture heated at 110 °C for 1 h. An ion-exchange resin was added to the solution after the heat treatment to remove excess ions.

Preparation of Pt-loaded WO_3 nanotubes: Different amounts of Pt colloidal solutions were added to samples of tungstic acid hydrate and the resulting mixtures stirred for 1 h at room temperature then dried in air at 60 °C. The solid products were heated from room temperature to 450 °C for 6 h and annealed at 450 °C for another 3 h to obtain the final yellow product. Commercial WO_3 particles were purchased from Kojundo Chemical Laboratory Co. Ltd. (Type: WWO04PB)

All materials were characterized by nitrogen cryosorption, SEM, and TEM. Details of the characterization and photocatalytic activity measurements are provided in the Supporting Information.

Received: May 12, 2008
Published online: July 28, 2008

Keywords: crystal growth · nanotubes · photocatalysis · platinum · tungsten

[1] A. Fujishima, K. Honda, *Nature* **1972**, *238*, 37–38.
[2] J. S. Hu, L. L. Ren, Y. G. Guo, H. P. Liang, A. M. Cao, L. J. Wan, C. L. Bai, *Angew. Chem.* **2005**, *117*, 1295–1299; *Angew. Chem. Int. Ed.* **2005**, *44*, 1269–1273.
[3] A. P. Finlayson, V. N. Tsaneva, L. Lyons, M. Clark, B. A. Glowacki, *Phys. Status Solidi A* **2006**, *203*, 327–335.
[4] S. C. Zhang, J. D. Shen, H. B. Fu, W. Y. Dong, Z. J. Zheng, L. Y. Shi, *J. Solid State Chem.* **2007**, *180*, 1456–1463.
[5] Y. Cong, J. L. Zhang, F. Chen, M. Anpo, *J. Phys. Chem. C* **2007**, *111*, 6976–6982.
[6] W. K. Ho, J. C. Yu, S. C. Lee, *Chem. Commun.* **2006**, *111*, 1115–1117.
[7] R. Asahi, T. Morikawa, T. Ohwaki, K. Aoki, Y. Taga, *Science* **2001**, *293*, 269–271.
[8] H. Irie, Y. Watanabe, K. Hashimoto, *J. Phys. Chem. B* **2003**, *107*, 5483–5486.
[9] Y. Cong, J. L. Zhang, F. Chen, M. Anpo, *J. Phys. Chem. C* **2007**, *111*, 6976–6982.
[10] G. R. Bamwenda, H. Arakawa, *Appl. Catal. A* **2001**, *210*, 181–191.
[11] R. Abe, H. Takami, N. Murakami, B. Ohtani, *J. Am. Chem. Soc.* **2008**, *130*, 7780–7781.
[12] L. S. Zhang, W. Z. Wang, Z. G. Chen, L. Zhou, H. L. Xu, W. Zhu, *J. Mater. Chem.* **2007**, *17*, 2526–2532.
[13] J. Wu, F. Duan, Y. Zheng, Y. Xie, *J. Phys. Chem. C* **2007**, *111*, 12866–12871.
[14] J. Zeng, H. Wang, Y. C. Zhang, M. K. Zhu, *J. Phys. Chem. C* **2007**, *111*, 11879–11887.
[15] J. Lin, J. Lin, Y. F. Zhu, *Inorg. Chem.* **2007**, *46*, 8372–8378.

[16] G. K. Mor, K. Shankar, M. Paulose, O. K. Varghese, C. A. Grimes, *Nano Lett.* **2005**, *5*, 191 – 195.
[17] H. X. Li, Z. F. Bian, J. Zhu, D. Q. Zhang, G. S. Li, Y. N. Huo, H. Li, Y. F. Lu, *J. Am. Chem. Soc.* **2007**, *129*, 8406 – 8407.
[18] L. F. Cheng, X. T. Zhang, Y. H. Chen, B. Liu, Y. C. Li, Y. B. Huang, Z. L. Du, *Chem. J. Chin. Univ.* **2004**, *25*, 1621 – 1623.
[19] L. F. Cheng, X. T. Zhang, Y. H. Chen, B. Liu, Y. C. Li, Y. B. Huang, Z. L. Du, *Chin. J. Inorg. Chem.* **2004**, *20*, 1117 – 1120.
[20] F. Chai, R. X. Tan, F. H. Cao, F. Y. Zhai, X. H. Wang, *Mater. Lett.* **2007**, *61*, 3939 – 3941.
[21] Y. Wu, Z. H. Xi, G. M. Zhang, J. Yu, D. Z. Guo, *J. Cryst. Growth* **2006**, *292*, 143 – 148.
[22] H. G. Choi, Y. H. Jung, D. K. Kim, *J. Am. Ceram. Soc.* **2005**, *88*, 1684 – 1686.
[23] R. Custelcean, *Chem. Commun.* **2008**, 295 – 307.
[24] F. A. Henglein, *J. Phys. Chem. B* **1997**, *101*, 5889 – 5894.
[25] Y. Ohko, A. Fujishima, K. Hashimoto, *J. Phys. Chem. B* **1998**, *102*, 2699 – 2704.

